ACS APPLIED MATERIALS & INTERFACES

Research Article

Cite This: ACS Appl. Mater. Interfaces 2019, 11, 42561−42570

www.acsami.org

Silver-Coated Poly(dimethylsiloxane) Beads for Soft, Stretchable, and Thermally Stable Conductive Elastomer Composites

Chengfeng Pan,[†,‡] Yunsik Ohm,[†,‡] Jingxian Wang,[§] Michael J. Ford,[†,‡] Kitty Kumar,[†,‡] Swarun Kumar,[§] and Carmel Majidi*[,†,‡,§,∥]

[†]Soft Machines Lab, [‡]Mechanical Engineering, [§]Electrical and Computer Engineering and [∥]Materials Science and Engineering, Carnegie Mellon University, Pittsburgh, Pennsylvania 15213, United States

Supporting Information

ABSTRACT: We introduce an elastomer composite filled with silver (Ag) flakes and Ag-coated poly(dimethylsiloxane) (PDMS) beads that exhibits electrical conductivity that is 2 orders of magnitude greater than that of elastomers in which the same concentration of Ag filler is uniformly dispersed. In addition to the dramatic enhancement in conductivity, these composites exhibit high mechanical compliance (strain limit, >100%) and robust thermal stability (conductivity change, <10% at 150 °C). The incorporation of Ag-coated PDMS beads introduces an effective phase segregation in which Ag flakes are confined to the "grain boundaries" between the embedded beads. This morphological control aids in the percolation of the Ag flakes and the formation of conductive bridges between neighboring Ag shells. The confinement of Ag flakes also suppresses thermal expansion and changes in electrical conductivity of the percolating networks when the composite is heated. We demonstrate potential applications of thermally stable elastic conductors in wearable devices and soft robotics by fabricating a highly stretchable antenna for a "smart" furnace glove and a strain sensor for soft gripper operation in hot water.

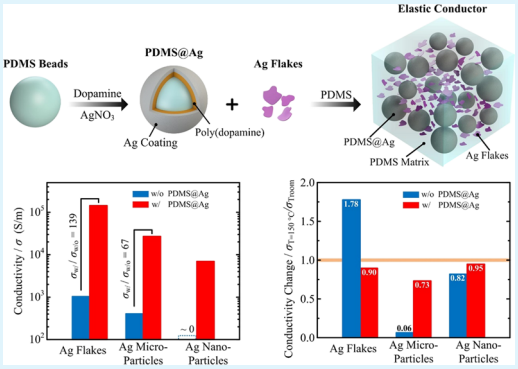

KEYWORDS: *silver-coated PDMS beads, stretchable and thermally stable conductor, soft robotics, wearable devices, stretchable electronics*

INTRODUCTION

Stretchable electronics have the potential for transformative impact for emerging applications in wearable computations,[1−8] soft robotics,[9−11] stretchable displays,[12−15] energy storage and harvesting devices,[16−21] and biocompatible devices.[22−26] Such technologies demand electrically conductive materials for robust circuit wiring along with mechanical compliance and deformability. Maintaining reliable electrical conductance during mechanical deformation can be achieved through a variety of techniques, including (i) wavy or serpentine microstructures of ultrathin silicon or metallic films[27,28] on an elastic substrate, (ii) soft microfluidics with conductive fluids such as gallium-based liquid metal alloy,[29,30] and (iii) electrically conductive polymers and gels.[31−33] Another common strategy for developing stretchable conductors is to disperse conductive fillers into an elastomer, resulting in a composite that combines the mechanical compliance of the polymer matrix with electrical conductivity enabled by a percolating network of conductive inclusions.[34−39] For instance, Matsuhisa et al.[35] presented a conductive ink that exhibited high conductivity (469 S/cm) and mechanical stretchability (>200% strain) enabled by dispersing silver flakes into a fluoropolymer matrix. Markvicka et al.[36] showed a liquid metal−elastomer composite with electrically "self-healing" properties due to the high mobility of the liquid metal droplets. Instead of using a single dispersion phase, some researchers have recently created composites with multiphase inclusions to achieve higher electrical conductivity with improved mechanical compliance and elasticity.[40−43] For instance, Wang et al.[41] introduced liquid metal particles into a composite that also contained silver flakes and an ethylene vinyl acetate (EVA) copolymer. This heterogeneous dispersion phase had extreme elasticity (>1000% strain) and high conductivity (8331 S/cm). Another approach toward stretchable conductors has been to create heterogeneous material architectures with controlled microstructures that reduce the content of conductive filler required to achieve target conductivity.[44−47] For example, Hu et al.[46] created a polymer composite composed of core−shell silver-coated polystyrene microspheres dispersed in a poly(dimethylsiloxane) (PDMS) matrix. With 42.88 wt % silver, they achieved an electrical conductivity of 412 S/cm, a conductivity that typically requires 74−85 wt % silver for composites with uniformly distributed fillers.[48,49] Similarly, Oh et al.[44] introduced ice spheres into a silver nanowire (AgNW) aqueous dispersion to produce a three-dimensional bimodal-porous AgNW nanostructure and

Received: July 26, 2019
Accepted: October 22, 2019
Published: October 22, 2019

DOI: 10.1021/acsami.9b13266
ACS Appl. Mater. Interfaces 2019, 11, 42561−42570

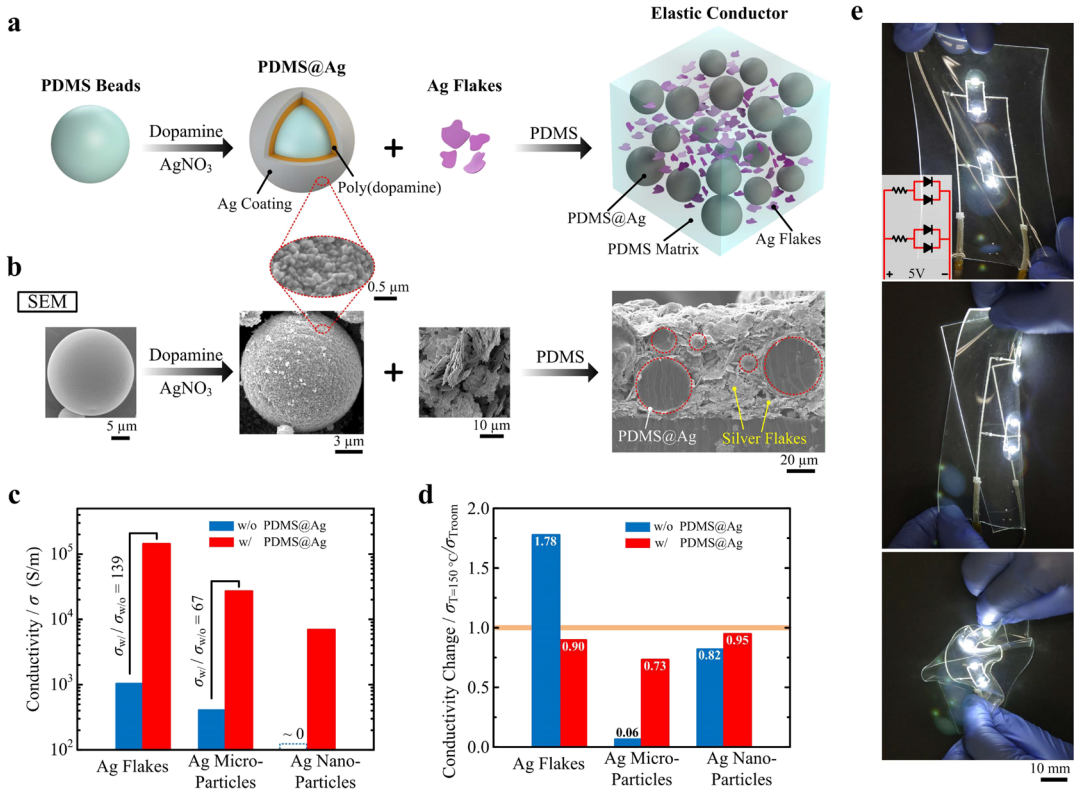

Figure 1. Thermally stable elastic conductors. (a) Schematic of the fabrication process of the elastic conductor from composite of silver (Ag)-coated PDMS beads (PDMS@Ag), Ag flakes as an example filler, and the PDMS matrix. PDMS@Ag is a core−shell structure consisting of a poly(dopamine) and a Ag shell. (b) Scanning electron microscopy (SEM) images corresponding to the previous illustration. The inset is the zoomed-in image of the Ag coating showing the Ag shell. (c) Electrical conductivity of elastic conductors from composites with different Ag fillers (Ag flakes, Ag microparticles, and Ag nanoparticles) with/without PDMS@Ag at a volumetric fraction of 12 vol % Ag. Composites with PDMS@Ag have around 2 orders of magnitude higher conductivity relative to composites without PDMS@Ag. (d) Electrical conductivity change of composites with/without PDMS@Ag between the temperature of 150 °C and room temperature. Composites with PDMS@Ag are more thermally stable in electrical conductivity. (e) Photographs of the stretchable LED circuitry made from a composite of PDMS@Ag and Ag flakes as the lead connection (red line in the inset) under stretching (top), folding (middle), and squeezing (bottom).

were able to achieve a 42 S/cm conductivity with only 2 wt % AgNW loading.

Another important, and often overlooked, requirement for stretchable conductive materials is robust thermal stability, that is, minimal influence of temperature on electrical resistance. Robust thermal stability is critical for heat-related applications such as microheaters and thermoelectric devices as well as resistance-sensitive devices such as resistive strain sensors. In general, the change in electrical resistance of conductive composites caused by increases in temperature is captured by the temperature coefficient of resistance (TCR). The increase or decrease in resistivity as temperature increases can be quantified with a positive temperature coefficient (PTC) or negative temperature coefficient (NTC) of resistance, respectively. Large TCR can cause device failure, can be a fire hazard, and/or can impair the operational reliability of an electronic system.[50] A common method for achieving low/near-zero TCR materials is to combine materials with different types of TCRs (positive and negative).[51] For instance, Chu et al.[50,52] reported a zero TCR hybrid consisting of alternating layers of carbon nanotube/PDMS (NTC) and carbon black/PDMS (PTC). However, these kinds of material architectures require layer-by-layer fabrication of the two types of materials, which is challenging to scale-up for mass manufacturing or for arbitrary form factors. An ideal conductive composite would have an intrinsically small TCR and not require special layups or geometries.

In this paper, we address these challenges with a core−shell silver-coated poly(dimethylsiloxane) (PDMS) (PDMS@Ag) bead-based materials architecture for elastic conductors that exhibits a dramatic enhancement in electrical conductivity, good thermal stability (i.e., small TCR), and high mechanical compliance. We studied the effects of the presence of PDMS@Ag on enhancement in electrical conductivity and suppression in the change of temperature-dependent conductivity relative to the composites without PDMS@Ag. The electromechanical properties of these conductive composites are also presented. Two potential applications of thermally stable elastic conductors for wearable devices and soft robotics were also demonstrated by a highly stretchable antenna for a "smart" furnace glove and a strain sensor for soft gripper operation in hot water.

RESULTS AND DISCUSSION

Phase-Segregated Silver−Silicone Composites (PS3). Referring to Figure 1a, the thermally stable elastic conductor is made from a phase-segregated composite composed of core−shell silver-coated poly(dimethylsiloxane) (PDMS; Sylgard 184, Dow Corning) (PDMS@Ag) beads and silver flakes dispersed in an elastic PDMS matrix. To facilitate bonding between the PDMS core and Ag shell, a poly(dopamine) layer

DOI: 10.1021/acsami.9b13266
ACS Appl. Mater. Interfaces 2019, 11, 42561−42570

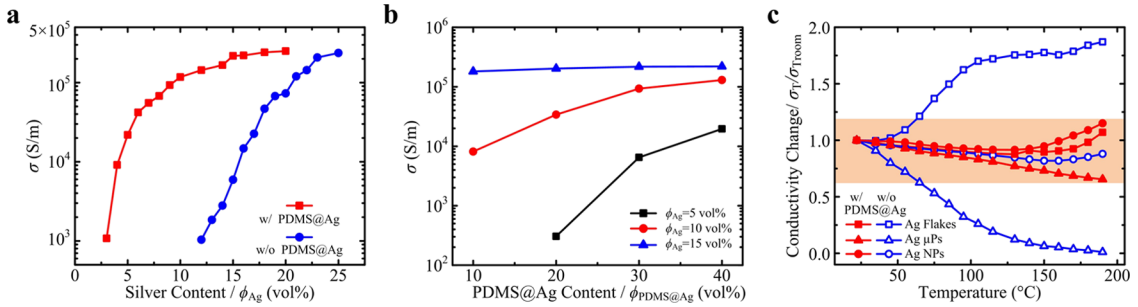

Figure 2. Electrical conductivity. (a) Conductivity of Ag−PDMS composites with/without PDMS@Ag beads as a function of total Ag content. The content of PDMS@Ag is fixed at 40 vol % for the composite with PDMS@Ag. (b) Conductivity of PDMS@Ag/Ag flake/PDMS as a function of PDMS@Ag content. (c) Electrical conductivity change of elastic conductors for composites with different Ag fillers (Ag flakes, Ag microparticles, and Ag nanoparticles) and with/without PDMS@Ag as a function of temperature. The shaded region highlights the relatively small deviation of conductivity as the temperature increases, which predominately occurs for composites with PDMS@Ag beads.

was coated on the PDMS beads prior to Ag deposition. The corresponding scanning electron microscopy (SEM) images (Figure 1b) show the Ag-coated PDMS microspheres (Figure S1) encased within a PDMS matrix. The Ag flakes are dispersed between the PDMS@Ag beads (Figure 1b), resulting in a local enhancement in Ag volumetric fraction and greater susceptibility to percolation. The incorporation of Ag-coated PDMS beads introduces an effective phase segregation in which Ag flakes are confined to the "grain boundaries" between the embedded beads. Henceforth, these phase-segregated silver-silicone material systems are referred to as PS3 composites. Moreover, the Ag shells on the PDMS@Ag beads establish additional sources of electrical connectivity between adjacent Ag flakes regions (alternatively, the percolating Ag flakes can be treated as conductive bridges between the Ag shells). The combination of these two effects, that is, local enhancement of the Ag flake content and the flakes−bead shells−flakes connectivity, enables the PS3 composite to achieve a 2 orders of magnitude (139×) enhancement in electrical conductivity (σ), compared to the uniformly dispersed Ag flake/PDMS composites with the same Ag content (12 vol %) (Figure 1c). This material architecture also works for other types of Ag fillers (Figures S2 and S3). The conductivity of a composite with PDMS@Ag and Ag microparticles is 67 times higher than a composite with only Ag microparticle fillers with the same Ag content (12 vol %). The conductivity of a composite with PDMS@Ag and Ag nanoparticles goes from being nonconductive ($\sigma \approx 0$) for a composite with only Ag nanoparticles to conductive ($\sigma = 6.94 \times 10^3$ S/m) (Figure 1c) at the same Ag content (12 vol %). Note that the total Ag content was determined by including the contribution from the PDMS@Ag shell. Since less Ag is needed to achieve the same electrical conductivity (1.4×10^5 S/m), this architecture enables a significant reduction in density compared to the uniformly dispersed Ag flake/PDMS composites (from 3.11 to 2.17 g/cm^3, i.e., 43.7% less). Last, the introduction of PDMS@Ag beads improves thermal stability of the conductivity (Figure 1d). We speculate that the similar thermal expansion of the PDMS beads and surrounding PDMS matrix results in a limited net impact on the percolating network of the Ag filler particles or their connectivity with the Ag shells. As shown in Figure 1e, a stretchable circuit powering an array of light-emitting diodes (LEDs) was fabricated using the PS3 composite with Ag flakes as the electrical leads (red lines in Figure 1e inset). The circuit maintained electrical functionality under mechanical deformation, for example, stretching, folding, and squeezing.

Electrical Conductivity. We first investigated the effects of PDMS@Ag on the conductivity of the composite by measuring conductivity as a function of total Ag content at fixed volumetric fractions of PDMS@Ag ($\phi_{PDMS@Ag}$ = 40 vol %) (Figure 2a). Conductivity of composites with and without PDMS@Ag increases as the silver content increases (ϕ_{Ag}). However, for the same silver content, the presence of PDMS@Ag leads to a significant increase in the electrical conductivity (up to 139 times). For example, with a low Ag content (3 vol %), we can engineer composites with PDMS@Ag inclusions that have an electrical conductivity greater than 10^3 S/m, whereas the composite without PDMS@Ag needs a 12 vol % Ag content. Likewise, highly conductive (1.17×10^5 S/m) PS3 composites can be achieved with ϕ_{Ag} = 10 vol %. For comparison, a Ag flake/PDMS composite with uniformly distributed filler particles requires ϕ_{Ag} = 21 vol % to achieve a similar conductivity (1.19×10^5 S/m). The spatial confinement and phase segregation of Ag-rich portions observed for PDMS@Ag promote percolation in these composites. As illustrated in Figure S4, the Ag flakes are confined to the grain boundaries between the PDMS@Ag inclusions. Thus, the actual volumetric fraction of Ag flakes in the PDMS matrix between PDMS@Ag beads is $\phi_{Ag/PDMS} = \phi_{Ag}/(1 - \phi_{PDMS@Ag})$, which explains the higher overall conductivity of the composite. In addition, the Ag shell layers that coat the PDMS@Ag beads provide continuous electrical connections between the percolating networks of Ag flakes that surround them. The distribution of PDMS@Ag beads aids in the formation of long-range conductive pathways throughout the entire composite. Figure 2b shows the conductivity of PS3 composites as a function of the PDMS@Ag content ($\phi_{PDMS@Ag}$) at fixed total volumetric fractions of silver (ϕ_{Ag} = 5, 10, and 15 vol %). For composites with low ϕ_{Ag} = 5 or 10 vol %, the conductivities dramatically increase with increasing $\phi_{PDMS@Ag}$. For ϕ_{Ag} = 15 vol %, the conductivity exhibits only a slight increase when adding PDMS@Ag due to the saturation of percolation pathways.

We then measured the electrical conductivity change of composites with and without PDMS@Ag as a function of temperature for different Ag fillers, that is, Ag flakes, Ag microparticles, and Ag nanoparticles (Figure 2c). We used 40 vol % PDMS@Ag along with 12 vol % total Ag content for all composites with PDMA@Ag inclusions. For each composite, we adjusted the amount of Ag fillers (i.e., 23 vol % for Ag flakes

DOI: 10.1021/acsami.9b13266
ACS Appl. Mater. Interfaces 2019, 11, 42561−42570

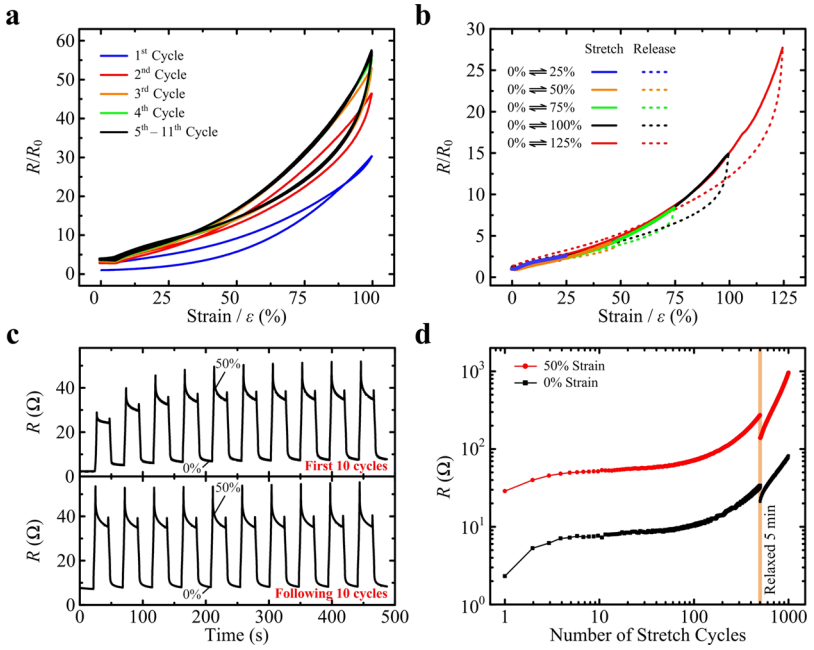

Figure 3. Electromechanical response of composites with PDMS@Ag beads and Ag flakes. (a) Normalized resistance as a function of strain up to 100% strain showing differences during the first four cycles and then convergence to the same curve for the 5th to 11th cycles. (b) Normalized resistance as a function of strain under different strain ranges. The data is collected after the conductor was precycled by stretching 10 times up to 100% strain. The results show negligible difference in the loading curves between stretching cycles but some hysteresis between loading and unloading within a stretching cycle. (c) Electromechanical response of the conductor when cyclically strained to 50% over 20 cycles (first 10 cycles-top following 10 cycles-bottom). (d) Resistance of the conductor at 50% elongation and relaxed states for over 1000 cycles. When the composite was held at a relaxed state for 5 min, it recovered some conductivity.

and 22 vol % for Ag microparticles and nanoparticles) so that they would have similar initial conductivities at room temperature. Unlike significant negative or positive temperature coefficients of resistance measured for Ag flake/PDMS or Ag microparticle/PDMS, respectively, the conductivities of composites with PDMS@Ag vary across a comparatively small range (highlighted in the plot), demonstrating thermally stable conductivity in the PDMS@Ag composites. For example, the conductivity of the PS3 composites changes by 7% when heated to 190 °C, whereas the increase for the Ag flake/PDMS composites is 87%. Generally, as temperature increases, the PDMS matrix expands. For anisotropic particles like Ag flakes, the thermal expansion of the surrounding PDMS may create additional percolating pathways and subsequently increase electrical conductivity. For isotropic particles like Ag microparticles, the thermal expansion of the surrounding PDMS can disrupt these percolating pathways and subsequently decreases electrical conductivity. With PDMS@Ag beads, additional Ag fillers are excluded from the volume that is occupied by the PDMS core of the bead. Thus, microstructural changes due to thermal expansion have less of an impact on percolation pathways in composites containing PDMS@Ag beads relative to composites with only Ag fillers.

The small particle size of Ag nanoparticles (<100 nm) results in low TCR for Ag nanoparticles/PDMS composites due to the close proximity between adjacent Ag nanoparticles, which limits the degradation of the percolating network from the thermal expansion of the surrounding PDMS matrix. Therefore, the addition of PDMS@Ag beads does not have a significant effect on further reducing the influence of temperature on electrical conductivity. Differential scanning calorimetry (DSC) (Figure S5) confirms no phase change of silver fillers for the composites with and without PDMS@Ag. As shown in Figure S6, the PS3 composites exhibit strong thermal stability (i.e., low change in electrical conductivity under cyclic heating and cooling). We also measured the conductivity change of elastic conductors with and without PDMS@Ag beads as temperature increased while the material was loaded in a stretched state. These results (Figure S7) also demonstrate the suppression effect of the PDMS@Ag beads and their ability to maintain thermal stability. In summary, the results in Figure 2 suggest that the material architecture of PDMS@Ag/Ag filler/PDMS composites exhibit a dramatic enhancement in electrical conductivity and robust thermal stability.

Electromechanical Properties. We then studied the electromechanical properties of the elastomer composite. For the results presented in Figure 3a–d, we used a PDMS@Ag content of 40 vol % and a Ag flake content of 15 vol % for all samples. A representative evolution of the relative change in resistance (R/R_0) of the PDMS@Ag/Ag flake/PDMS composite as a function of the tensile strain (ε) for 11 cyclic stretching and releasing cycles up to ε = 100% is presented in Figure 3a. The results show hysteresis in the electromechanical response for the first four cycles and then converge to identical responses from the 5th to 11th cycles. We measured the mechanical response under different tensile strain ranges (Figure 3b) after precycling to ε = 100% for 10 cycles. In the first cycle following precycling, the sample was first stretched by 25% and then relaxed to its original length. In each consecutive cycle, the strain was increased by steps of 25% up to ε = 125%. The normalized resistance as a function of strain overlaps for each subsequent cycle with reasonable agreement. We observe some modest hysteresis between loading and unloading of each strain cycle. The representative stress–strain curves (Figure S8a) indicate that the strain limit of PS3

DOI: 10.1021/acsami.9b13266
ACS Appl. Mater. Interfaces 2019, 11, 42561–42570

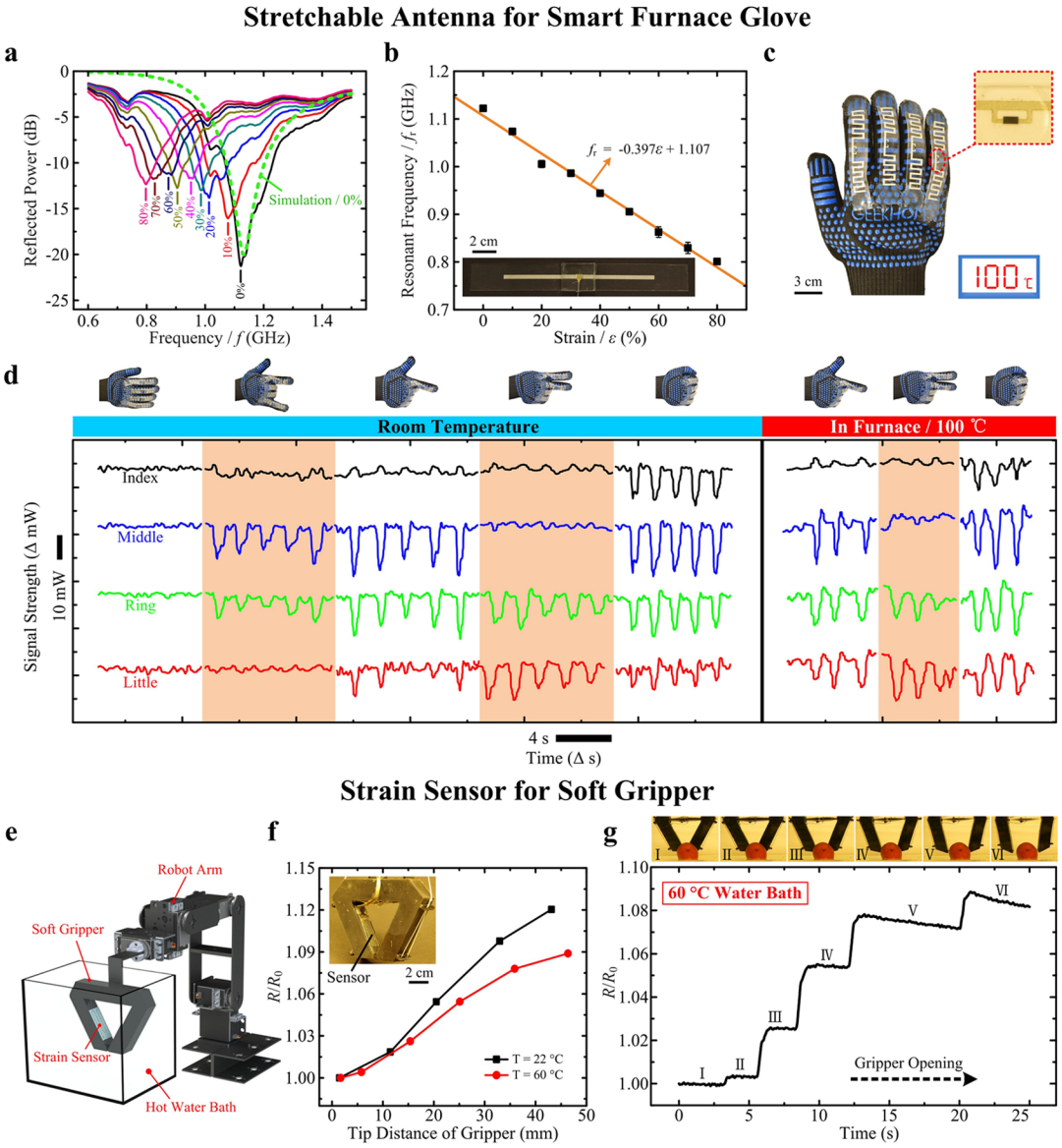

Figure 4. Applications of thermally stable elastic conductors as a stretchable antenna and strain sensor for wearable devices and soft robotics. (a–d) Stretchable antenna: (a) frequency response of the reflected power from a representative antenna sample at different strains. The green dashed curve is the simulation result at the initial length, which is in strong agreement with the experimental result. (b) Resonant frequency (f_r) of the antenna as a function of strain. The inset is a photograph of the antenna. (c) Photograph of the sensorized furnace glove with stretchable RF tags (white serpentine). The inset shows the integrated RF chip. (d) Posture recognition of five different gestures of the hand in room-temperature (left) and furnace environment (high temperature) (right). The scale bars of axes are shown beside the axes. The photographs are the posture for each time window. (e–g) Strain sensor for the soft gripper: (e) schematic illustration of the strain sensor on a soft gripper-mounted robot arm. (f) Resistance response of the strain sensor as a function of the tip distance of the gripper in room-temperature and hot water baths (~60 °C). The inset is the photograph of the sensor-integrated soft gripper. (g) Resistance response of the strain sensor during the gripper opening for the task of food capture in hot water. The photographs of the gripper correspond to each opening state.

composites is larger than 100%. The composites will maintain electrically conductive until mechanical breakdown (Figure S8b). As shown in Figure 3c, the PS3 conductors demonstrate a largely consistent electromechanical behavior; that is, after an initial rise, the resistance profile is constant when cyclically strained between ε = 0 and 50% over 20 loading cycles. The resistance profile converges to identical pulses after four cycles, which is consistent with the results in Figure 3a. The long-term use of this elastic conductor is evaluated by performing cyclic loading up to 50% strain (Figure 3d). After an initial break-in period (5cycles), the electromechanical response stabilizes and is repeatable for the following 10 cycles. During subsequent stretching cycles, we observe that the resistance in both the relaxed and 50% elongated states begins to increase significantly after ~50 cycles. After 500 cycles, the conductor was held at a relaxed state for 5 min (orange line), and the resistance is observed to decrease, suggesting some recovery of the conductivity due to the local stress release causing the reconfiguration of conductive pathways. This trend of resistance change during cyclic loading is common for many particle-filled composites.[40] Nonetheless, there remains room to improve the performance of the PS3 composites for high cyclical loading, such as adding surfactants for better bonding between the conductive filler and matrix[35] or with the

DOI: 10.1021/acsami.9b13266
ACS Appl. Mater. Interfaces 2019, 11, 42561–42570

inclusion of liquid metal for reducing internal stress concentrations.[41] Despite the resistance increase during cyclic loading, the PDMS@Ag-based elastic conductors demonstrate high stretchability and relatively robust electromechanical performance.

Applications: Stretchable Antenna and Strain Sensor. To demonstrate the potential applications of the conductive PS3 composites, we present two representative use cases related to wearable computation and soft robotics. The first example (Figure 4a−d) is a sensorized furnace glove that can withstand elevated temperatures. The PS3 composite functions as a stretchable radiofrequency (RF) antenna for measuring and transmitting strain information through coupling between antenna resonance and mechanical tensile strain. Two rectangular-shaped dipole antennas (53.9 mm × 3 mm × 0.14 mm) were fabricated on a PDMS substrate by stencil printing with a gap distance of 2.3 mm. A coaxial male connector (uFL SMT antenna connector, Adafruit) with a coaxial cable (RN-uFL-SMA6, Digi-key) was mounted to the antennas with silver epoxy. Another PDMS layer was applied to encapsulate and protect the antennas and the electrical contact between the antennas and connector (see Figure 4b inset and Figure S9). Representative measurements of the reflected power as a function of frequency under different strains are shown in Figure 4a. We performed simulations in ANSYS and designed the antennas to have a resonance frequency of ∼1.1 GHz at 0% strain (see the Supporting Information in Section S1 for simulation details). The simulation is in (green dashed line; Figure 4a) good agreement with the experimental measurements (black line; Figure 4a). Figure 4a shows the shift of resonance frequency (valley point) and a similar level of high-quality radiation efficiency, that is, low enough reflected power, as the elongation of antennas up to 80% strain. The resonant frequency of the antenna as a function of strain is presented in Figure 4b. The resonant frequency (f_r) decreases linearly from 1.12 to 0.80 GHz as the sample was stretched to ε = 80% with a linear fitting of f_r = (-0.397ε + 1.107) GHz with R^2 = 0.99. These results show the tunability of the stretchable antenna made from the PS3 composite over a wide range of frequencies. Since the resonant frequency of the antenna is linearly dependent on the strain, the antennas can function in a sensorized furnace glove.

To demonstrate the practical capabilities of the stretchable antenna for wearable devices, we produced an RFID-integrated smart furnace glove (Figure 4c) for monitoring hand gestures in a high-temperature environment. The glove contains four stretchable antenna-integrated RFID tags over the metacarpophalangeal, proximal, and distal interphalangeal joints of each finger (excluding the thumb; find the design of the RFID tag in Figure S10). We show the thermally stable functionality of this smart glove by recognizing a series of hand gestures in room temperature and high temperature (in a 100 °C furnace) (Figure 4d). In these experiments, the fingers are cycled through different gestures where the signal strength of each individual RFID tag is captured by a far-field RFID antenna (LHCP far-field RFID antenna, Impinj) and reader system (speedway revolution R240 UHF RFID reader, Impinj) using an integrated RF chip. The scanning frequency is from 0.902 to 0.928 GHz. As shown in the left part of Figure 4d (room temperature operation), the signal strength of the RFID tag will decrease from the baseline when the corresponding finger is bent. The high-temperature tests (Figure 4d, right and Movie S1) were performed in an ∼100 °C furnace and showed a similar decrease from the baseline when the corresponding finger was bent when compared to room-temperature measurements. The PS3 composites permit robust functionality of RFID tags, that is, gestures recognition, in a high-temperature environment.

The potential of the PS3 conductor in soft robotic applications is demonstrated with a strain sensor that is integrated into a robotic gripper that lifts food out of hot water. As shown in Figure 4e, the gripper system is assembled on a 4 degree of freedom robot arm (UARM Swift Pro, UFactory). Two cables driven by stepper motors were used to open and close the soft gripper. We use the same soft gripper made of silicone rubber as in our previous work.[53] A strain sensor fabricated with a PDMS@Ag/Ag flake/PDMS composite (Figure S11) was mounted on the inner side of the soft gripper to monitor the bending of the gripper jaw. The opening of the gripper jaw causes the strain sensor to elongate, increasing electrical resistance. The relative resistance (R/R_0) can be monitored as a function of the tip distance of the gripper in room-temperature and hot water bath (60 °C; Figure 4f). As with the furnace glove, the results here show that the strain sensor works similarly in high-temperature and room-temperature environments. The process of grasping a food object (red potato) in a bath of hot water (60 °C) is presented in Movie S2. Figure 4g shows the relative resistance change of the strain sensor during the gripper opening. Referring to the top of the figure, each signal increase corresponds to a turn of the stepper motor that is pulling the cable. Strain sensors for a robotic gripper along with the sensorized furnace glove demonstrate the potential of the PS3 composite in the applications of wearable computation and soft robotic in both mild- and high-temperature environments.

CONCLUSIONS

We have introduced a new material architecture for elastic conductors that exhibit a combination of high electrical conductivity with low conductive filler (silver) content, robust thermal stability (small TCR), and high mechanical compliance (strain limit >100%). The conductive elastomers are made from composites composed of core−shell Ag-coated elastomer microspheres (PDMS@Ag), Ag fillers (Ag flakes, Ag microparticles, and Ag nanoparticles), and an elastic matrix (PDMS). The presence of PDMS@Ag beads improves the electrical conductivity for two reasons. First, Ag fillers that form percolation pathways are sterically confined to regions between adjacent PDMS@Ag beads, resulting in effective phase segregation and a highly localized increase in the density of Ag filler particles. Second, the Ag shells that coat the PDMS microspheres function as additional conductive pathways that connect the percolating networks formed within the surrounding Ag-rich domains. We postulate that the enhanced thermal stability is enabled by the presence of elastomer cores of the PDMS@Ag beads. With PDMS@Ag beads, additional Ag fillers are excluded from the volume that is occupied by the PDMS core of the bead. Thus, microstructural changes due to thermal expansion have less of an impact on percolation pathways in composites containing PDMS@Ag beads relative to those with only Ag fillers. The enhanced thermal stability of PS3 composites relative to composites without PDMS@Ag beads enables soft electronics to be used in high-temperature environments that arise in manufacturing, materials handling, and cooking. We demonstrated specific examples where the PS3 composite could be used by fabricating a sensorized

DOI: 10.1021/acsami.9b13266
ACS Appl. Mater. Interfaces 2019, 11, 42561−42570

furnace glove and a soft gripper for use in high-temperature environments. Further efforts could extend this phase-segregated material architecture to other types of polymers, filler particles, and coatings while focusing on niche applications where high-temperature stability, electrical conductivity, and deformability are necessitated.

EXPERIMENTAL SECTION

Core−Shell PDMS@Ag Preparation. To synthesize poly(dimethylsiloxane) (PDMS) microspheres, 10 g of uncured PDMS (10:1 ratio of base to curing agent, Sylgard 184, Dow Corning) was first added into poly(vinyl alcohol) (PVA 3 wt %, Ward's Science) using a syringe pumping system (PHD 4400, Harvard Apparatus) with an infusion speed of 1 mL/min and a needle size of 18 G. During the infusing process, the PVA solution was magnetically stirred at 1000 rpm. Probe sonication (Vibra-Cell VC250, Sonics & Materials Inc.) was next used at 100% power for 1 h to break down the millimeter-sized PDMS droplets into microspheres. The PVA solution was merged in an ice bath during infusion and sonicated to prevent the curing of PDMS. Next, the liquid PDMS microspheres were cured at 70 °C for 6 h in the PVA solution. The solid PDMS beads were collected by centrifuging at 5000 rpm and then rinsed with Tris base buffer (10 mM; Sigma-Aldrich) three times with a centrifuge. For the poly(dopamine) (PDA) coating, we dispersed 10 g of cross-linked PDMS beads and 0.4 g of dopamine hydrochloride (Sigma-Aldrich) into 200 mL of Tris base buffer solution. The solution was magnetically stirred at 350 rpm for 24 h at room temperature to coat PDMS beads with the PDA layer. To remove the unreacted dopamine, the PDMS@PDA beads were washed with Tris base buffer three times by centrifuging with a speed of 5000 rpm. Then, we used an electroless plating process to coat PDMS@PDA with a silver layer. To do this, we dispersed PDMS@PDA beads (10 g) and 3.6 g of silver nitrate ($AgNO_3$, Salt Lake Metals) in 100 mL of Tris base buffer. The light-sensitive solution was magnetically stirred (125 rpm) for 1.5 h at room temperature in a dark environment to form a seed layer of silver. After this, we added 200 mL of ascorbic acid (L-ascorbic acid, Sigma-Aldrich) solution to facilitate the reduction of silver for 5 min to form core−shell PDMS@Ag beads. The initial concentration of ascorbic acid solution was 46.5 mg/mL in Tris base buffer, that is, 9.3 g of ascorbic acid in 200 mL of Tris base buffer. The PDMS@Ag beads were rinsed with deionized water and then isopropyl alcohol (IPA; >99.7%, Sigma-Aldrich) three times. Finally, PDMS@Ag was obtained after drying in a vacuum oven at 80 °C.

PDMS@Ag/Ag Filler/PDMS Composite Preparation. The PDMS@Ag beads, Ag filler, uncured PDMS matrix, and methyl isobutyl ketone (MIBK; Sigma-Aldrich) were added into a 20 mL glass vial and then placed into a planetary THINKY mixer where they were mixed for 2 min. The uncured PDMS matrix was also prepared using the THINKY, which was used to mix the two-part polymers (10:1 ratio of base to the curing agent) for 1 min. The Ag fillers we use in this study are Ag flakes (size: 2−5 μm, Inframat Advanced Materials), Ag microparticles (2−3.5 μm powder, >99.9% trace metals basis, Sigma-Aldrich), and silver nanoparticles (<100 nm nanopowder, >99.5% trace metals basis, Sigma-Aldrich). We calculate the volumetric fraction of Ag based on 10.5 g/mL for the Ag density, 1.03 g/mL for the PDMS density, and an estimated 1.24 g/mL for the density of the PDMS@Ag particles assuming full reduction to Ag of the $AgNO_3$ coating (2.29 g) on the PDMS particles (10 g). The actual density may be smaller if Ag is not fully reduced. The total volumetric fraction is calculated from the cumulative amount of Ag in both the PDMS@Ag beads and filler within the PS3 composite.

Conductivity Test. A substrate film of PDMS (~400 μm) was created from uncured PDMS using a thin film applicator (ZUA 2000.150, Zehntner) on a flat surface (glass sheet or stainless steel sheet for temperature-related tests) and placed into an oven at 100 °C for 1 h to cure the substrate. Then, the PDMS@Ag/Ag filler/PDMS composite ink was printed on a PDMS substrate using stencil printing. The stencil mask (LaserTape, IKONICS Imaging) was fabricated with a laser cutter (VLS3.50, Universal Laser System) with settings of 100% speed, 100% power, and 1000 ppi. After printing, samples were placed in a room-temperature environment for 30 min for solvent evaporation and then moved to a 100 °C oven for 12 h to cure. For each test case, we printed four samples with 40 mm × 1.5 mm × 0.14 μm traces that terminated with 5 mm × 5 mm pads at each end. The electrical resistance of each sample was measured with a micro-ohm meter (HP 34420A, Hewlett-Packard) using a four-probe method in which probes were inserted into liquid metal droplets deposited on the terminal pads. For measuring conductivity as a function of temperature, we used a hot plate to manually control the temperature of the sample with an infrared thermometer (62 Mini IR Thermometer, Fluke). For the temperature-dependent conductivity measurement, we used a custom-made acrylic holder to perform five consecutive tensile loads (strain, ~0, 25, 50, 75, and 100%) and used an aluminum block as the thermal connector between the hot plate and specimen.

Electromechanical Test. We characterized the electromechanical properties of PDMS@Ag/Ag flake/PDMS composites that contained 40 vol % PDMS@Ag beads and 15 vol % Ag flakes. Samples were prepared in a dog bone geometry (ASTM D638v) and tested using a materials testing system (5969, Instron) at a strain rate of 2 mm/s for the tests shown in Figure 3a,b and 10 mm/s for the tests shown in Figure 3c,d. The conductive trace, that is, PDMS@Ag/Ag flake/PDMS composite, was printed on a PDMS substrate (~400 μm) at the dog bone center with trace dimensions of 85 mm × 1.5 mm × 0.14 mm and pad dimensions of 5 mm × 5 mm at each end. Two conductive fabric strips (Sparkfun Electronics) were connected to the ends of the cured composite via a small droplet of liquid metal. Another PDMS layer (~500 μm) was used to encapsulate the conductive trace and connections between the fabric strips and conductive trace. The sample was cut into a dog bone shape using a laser cutter (VLS3.50, Universal Laser System) with settings of 100% speed, 100% power, 1000 ppi, and four times repetition. The external analog data from the materials testing machine (5969 Instron) and voltage signal from the voltage divider circuit were collected using a USB DAQ (USB-6002, NI) with a sampling rate of 200 Hz through the serial interface (MATLAB, 2016a).

Stretchable Antenna. For the characterization of antenna performance under mechanical tensile strain, two rectangle-shaped dipole antennas were printed on a PDMS substrate. A coaxial male connector (uFL SMT antenna connector, Adafruit) with a coaxial cable (RN-uFL-SMA6, Digi-key) was mounted to antennas with a silver-filled conductive epoxy (H20E, World Precision Instruments). The epoxy was cured by heating in an oven at 100 °C for 1 h. The silver epoxy provides robust electrical and mechanical connections between the terminals of the soft PS3 traces and the pins of the rigid RF chip. Another PDMS layer was applied to encapsulate the sample. The design of the antenna and the geometry of the sample can be found in the Supporting Information. A vector network analyzer (ZVC Vector Network Analyzer, Rohde & Schwarz) was used to measure the reflected power of antenna as a function of frequency scanned from 0.6 to 1.5 GHz. We used an acrylic stretcher to apply a discrete mechanical deformation of 0, 10, 20, 30, 40, 50, 60, 70, and 80% strain. A finite element method solver (HFSS, ANSYS) simulated the reflected power of the antenna at 0% strain (see details in the Supporting Information). For the smart glove, four RFID tags with stretchable antennas were glued on the fingers of the furnace glove by Sil-Poxy. On each RFID tag, an RFID chip (LXMS31ACNA-009, Murata Electronics North America) was mounted between the two antennas. The fabrication process of the tag is the same as previous antenna samples, and its design is presented in the Supporting Information. During gesture recognition experiments, a far-field RFID antenna (LHCP far-field RFID antenna, Impinj) and a reader system (speedway revolution R240 UHF RFID reader, Impinj) were used to detect the signal strength of the individual RFID tag. A self-made software (wrote with Python) was used to collect and visualize the data. For the gesture recognition in high temperature, a furnace was used to provide the high-temperature environment. The initial temperature was set as 100 °C.

DOI: 10.1021/acsami.9b13266
ACS Appl. Mater. Interfaces 2019, 11, 42561−42570

Strain Sensor. The printing of the strain sensor and the assembly of the electrical connectors (conductive fabric strips) are the same as previously described in the Electromechanical Test section. The design of the strain sensor can be found in the Supporting Information. The strain sensor was glued at the inner side of the soft gripper with Sil-Poxy (Smooth-On) at room temperature for 6 h. The operation of the gripper (opening and closing) was manually controlled by two-step motors and fabric strings through an Arduino board. The whole gripper system was mounted on a 4 degree of freedom robot arm (UARM Swift Pro, UFactory) to orient the gripper. The distance of the gripper tip was measured through a filmed video and image processing. For the hot water grasping operation, the soft gripper with the sensor was immersed in a 60 °C water bath and used to grasp a red potato. Grasping was manually controlled through the software used to activate stepper motors for driving the cables attached to the robot fingers. The water bath was heated by a hot plate using a temperature-probe control.

■ ASSOCIATED CONTENT

Supporting Information

The Supporting Information is available free of charge on the ACS Publications website at DOI: 10.1021/acsami.9b13266.

Antenna design and simulation (Section S1); supporting figures (Section S2): SEM images of polydisperse core−shell PDMS and PDMS@Ag beads (Figure S1), SEM image of Ag fillers (Figure S2), SEM images of the cross section of the PS3 composite (Figure S3), 2D schematic illustration of the comparison between Ag/PDMS and PS3 composite showing the phase segregation of Ag flakes between PDMS@Ag grains (Figure S4), DSC measurements of Ag/PDMS and PS3 composites (Figure S5), electrical conductivity change of elastic conductors for composites with/without PDMS@Ag as a function of cyclic temperature loading (Figure S6), electrical conductivity change of elastic conductors for composites with/without PDMS@Ag as a function of temperature at different strains (Figure S7), stress−strain curves and resistance change as a function of strain until mechanical failure of PS3 composites with Ag flakes (Figure S8), the design schematic and photograph of stretchable antenna for vector network analyzing (Figure S9), the design schematic and photograph of the RFID tag for the smart glove (Figure S10), and the design schematic and photograph of the strain sensor (Figure S11) (PDF)

Supporting videos (Section S3): stretchable antenna for the smart furnace glove (Movie S1) (MP4)

Strain sensor for the soft gripper used in hot water (Movie S2) (MP4)

■ AUTHOR INFORMATION

Corresponding Author

*E-mail: cmajidi@andrew.cmu.edu.

ORCID

Chengfeng Pan: 0000-0001-8825-8011

Carmel Majidi: 0000-0002-6469-9645

Author Contributions

C.P., Y.O., M.J.F., K.K., and C.M. designed the experiments and formulated the ideas; C.P., Y.O., J.W., and K.K. performed the research; C.P., Y.O., J.W., M.J.F., K.K., S.K., and C.M analyzed and interpreted the data; and C.P., Y.O., J.W., M.J.F., K.K., S.K., and C.M. wrote the paper.

Notes

The authors declare no competing financial interest.

■ ACKNOWLEDGMENTS

The authors thank Dr. Mohammad H. Malakooti for help with differential scanning calorimetry. This work was supported by the National Science Foundation CMMI program (Civil, Mechanical, and Manufacturing Innovation; Dr. Mary M. Toney; award 1,635,824).

■ REFERENCES

(1) Kim, C.-C.; Lee, H.-H.; Oh, K. H.; Sun, J.-Y. Highly Stretchable, Transparent Ionic Touch Panel. *Science* **2016**, *353*, 682−687.

(2) Son, D.; Kang, J.; Vardoulis, O.; Kim, Y.; Matsuhisa, N.; Oh, J. Y.; To, J. W. F.; Mun, J.; Katsumata, T.; Liu, Y.; McGuire, A. F.; Krason, M.; Molina-Lopez, F.; Ham, J.; Kraft, U.; Lee, Y.; Yun, Y.; Tok, J. B.-H.; Bao, Z. An Integrated Self-healable Electronic Skin System Fabricated Via Dynamic Reconstruction of A Nanostructured Conducting Network. *Nat. Nanotechnol.* **2018**, *13*, 1057.

(3) Chortos, A.; Liu, J.; Bao, Z. Pursuing Prosthetic Electronic Skin. *Nat. Mater.* **2016**, *15*, 937.

(4) Jin, H.; Matsuhisa, N.; Lee, S.; Abbas, M.; Yokota, T.; Someya, T. Enhancing the Performance of Stretchable Conductors for E-Textiles by Controlled Ink Permeation. *Adv. Mater.* **2017**, *29*, 1605848.

(5) Kim, K. K.; Hong, S.; Cho, H. M.; Lee, J.; Suh, Y. D.; Ham, J.; Ko, S. H. Highly Sensitive and Stretchable Multidimensional Strain Sensor with Prestrained Anisotropic Metal Nanowire Percolation Networks. *Nano Lett.* **2015**, *15*, 5240−5247.

(6) Lipomi, D. J.; Vosgueritchian, M.; Tee, B. C.-K.; Hellstrom, S. L.; Lee, J. A.; Fox, C. H.; Bao, Z. Skin-like Pressure and Strain Sensors Based on Transparent Elastic Films of Carbon Nanotubes. *Nat. Nanotechnol.* **2011**, *6*, 788.

(7) Kwon, D.; Lee, T.-I.; Shim, J.; Ryu, S.; Kim, M. S.; Kim, S.; Kim, T.-S.; Park, I. Highly Sensitive, Flexible, and Wearable Pressure Sensor Based on a Giant Piezocapacitive Effect of Three-Dimensional Microporous Elastomeric Dielectric Layer. *ACS Appl. Mater. Interfaces* **2016**, *8*, 16922−16931.

(8) Segev-Bar, M.; Landman, A.; Nir-Shapira, M.; Shuster, G.; Haick, H. Tunable Touch Sensor and Combined Sensing Platform: Toward Nanoparticle-based Electronic Skin. *ACS Appl. Mater. Interfaces* **2013**, *5*, 5531−5541.

(9) Liu, Z. F.; Fang, S.; Moura, F. A.; Ding, J. N.; Jiang, N.; Di, J.; Zhang, M.; Lepró, X.; Galvao, D. S.; Haines, C. S.; Yuan, N. Y.; Yin, S. G.; Lee, D. W.; Wang, R.; Wang, H. Y.; Lv, W.; Dong, C.; Zhang, R. C.; Chen, M. J.; Yin, Q.; Chong, Y. T.; Zhang, R.; Wang, X.; Lima, M. D.; Ovalle-Robles, R.; Qian, D.; Lu, H.; Baughman, R. H. Hierarchically Buckled Sheath-core Fibers for Superelastic Electronics, Sensors, and Muscles. *Science* **2015**, *349*, 400−404.

(10) Keplinger, C.; Sun, J.-Y.; Foo, C. C.; Rothemund, P.; Whitesides, G. M.; Suo, Z. Stretchable, Transparent, Ionic Conductors. *Science* **2013**, *341*, 984−987.

(11) Hines, L.; Petersen, K.; Lum, G. Z.; Sitti, M. Soft Actuators for Small-scale Robotics. *Adv. Mater.* **2017**, *29*, 1603483.

(12) Larson, C.; Peele, B.; Li, S.; Robinson, S.; Totaro, M.; Beccai, L.; Mazzolai, B.; Shepherd, R. Highly Stretchable Electroluminescent Skin for Optical Signaling and Tactile Sensing. *Science* **2016**, *351*, 1071−1074.

(13) Sekitani, T.; Nakajima, H.; Maeda, H.; Fukushima, T.; Aida, T.; Hata, K.; Someya, T. Stretchable Active-matrix Organic Light-emitting Diode Display Using Printable Elastic Conductors. *Nat. Mater.* **2009**, *8*, 494.

(14) Stauffer, F.; Tybrandt, K. Bright Stretchable Alternating Current Electroluminescent Displays Based on High Permittivity Composites. *Nat. Mater.* **2016**, *28*, 7200−7203.

(15) Liang, J.; Li, L.; Niu, X.; Yu, Z.; Pei, Q. Elastomeric Polymer Light-emitting Devices and Displays. *Nat. Photonics* **2013**, *7*, 817.

(16) Chiba, S.; Waki, M.; Wada, T.; Hirakawa, Y.; Masuda, K.; Ikoma, T. Consistent Ocean Wave Energy Harvesting Using Electroactive Polymer (Dielectric Elastomer) Artificial Muscle Generators. *Appl. Energy* **2013**, *104*, 497−502.
(17) Li, Q.; Chen, L.; Gadinski, M. R.; Zhang, S.; Zhang, G.; Li, H. U.; Iagodkine, E.; Haque, A.; Chen, L.-Q.; Jackson, T. N.; Wang, Q. Flexible High-temperature Dielectric Materials from Polymer Nanocomposites. *Nature* **2015**, *523*, 576.
(18) Li, Q.; Zhang, G.; Liu, F.; Han, K.; Gadinski, M. R.; Xiong, C.; Wang, Q. Solution-Processed Ferroelectric Terpolymer Nanocomposites with High Breakdown Strength and Energy Density Utilizing Boron Nitride Nanosheets. *Energy Environ. Sci.* **2015**, *8*, 922−931.
(19) Lipomi, D. J.; Bao, Z. Stretchable, Elastic Materials and Devices for Solar Energy Conversion. *Energy Environ. Sci.* **2011**, *4*, 3314−3328.
(20) Xie, Y.; Yu, Y.; Feng, Y.; Jiang, W.; Zhang, Z. Fabrication of Stretchable Nanocomposites with High Energy Density and Low Loss from Cross-linked PVDF Filled with Poly (dopamine) Encapsulated $BaTiO_3$. *ACS Appl. Mater. Interfaces* **2017**, *9*, 2995−3005.
(21) Pan, C.; Markvicka, E. J.; Malakooti, M. H.; Yan, J.; Hu, L.; Matyjaszewski, K.; Majidi, C. A Liquid-Metal−Elastomer Nanocomposite for Stretchable Dielectric Materials. *Adv. Mater.* **2019**, *31*, 1900663.
(22) Kim, D.-H.; Lu, N.; Ma, R.; Kim, Y.-S.; Kim, R.-H.; Wang, S.; Wu, J.; Won, S. M.; Tao, H.; Islam, A.; Yu, K. J.; Kim, T.-i.; Chowdhury, R.; Ying, M.; Xu, L.; Li, M.; Chung, H.-J.; Keum, H.; McCormick, M.; Liu, P.; Zhang, Y.-W.; Omenetto, F. G.; Huang, Y.; Coleman, T.; Rogers, J. A. Epidermal Electronics. *Science* **2011**, *333*, 838−843.
(23) Park, J.; Choi, S.; Janardhan, A. H.; Lee, S.-Y.; Raut, S.; Soares, J.; Shin, K.; Yang, S.; Lee, C.; Kang, K.-W.; Cho, H. R.; Kim, S. J.; Seo, P.; Hyun, W.; Jung, S.; Lee, H.-J.; Lee, N.; Choi, S. H.; Sacks, M.; Lu, N.; Josephson, M. E.; Hyeon, T.; Kim, D.-H.; Hwang, H. J. Electromechanical Cardioplasty Using a Wrapped Elasto-Conductive Epicardial Mesh. *Sci. Transl. Med.* **2016**, *8*, 344ra86.
(24) Choi, S.; Han, S. I.; Jung, D.; Hwang, H. J.; Lim, C.; Bae, S.; Park, O. K.; Tschabrunn, C. M.; Lee, M.; Bae, S. Y.; Yu, J. W.; Ryu, J. H.; Lee, S.-W.; Park, K.; Kang, P. M.; Lee, B. W.; Nezafat, R.; Hyeon, T.; Kim, D.-H. Highly Conductive, Stretchable and Biocompatible Ag−Au Core−sheath Nanowire Composite for Wearable and Implantable Bioelectronics. *Nat. Nanotechnol.* **2018**, *13*, 1048−1056.
(25) Kim, S. H.; Jung, S.; Yoon, I. S.; Lee, C.; Oh, Y.; Hong, J. M. Ultrastretchable Conductor Fabricated on Skin-Like Hydrogel−Elastomer Hybrid Substrates for Skin Electronics. *Adv. Mater.* **2018**, *30*, 1800109.
(26) Wang, Z.; Huang, Y.; Sun, J.; Huang, Y.; Hu, H.; Jiang, R.; Gai, W.; Li, G.; Zhi, C. Polyurethane/Cotton/Carbon Nanotubes Core-Spun Yarn as High Reliability Stretchable Strain Sensor for Human Motion Detection. *ACS Appl. Mater. Interfaces* **2016**, *8*, 24837−24843.
(27) Rogers, J. A.; Someya, T.; Huang, Y. Materials and Mechanics for Stretchable Electronics. *Science* **2010**, *327*, 1603−1607.
(28) Kim, D.-H.; Song, J.; Choi, W. M.; Kim, H.-S.; Kim, R.-H.; Liu, Z.; Huang, Y. Y.; Hwang, K.-C.; Zhang, Y.-w.; Rogers, J. A. Materials and Noncoplanar Mesh Designs for Integrated Circuits with Linear Elastic Responses to Extreme Mechanical Deformations. *Proc. Natl. Acad. Sci. U. S. A.* **2008**, *105*, 18675−18680.
(29) Pan, C.; Kumar, K.; Li, J.; Markvicka, E. J.; Herman, P. R.; Majidi, C. Visually Imperceptible Liquid-Metal Circuits for Transparent, Stretchable Electronics with Direct Laser Writing. *Adv. Mater.* **2018**, *30*, 1706937.
(30) Dickey, M. D. Stretchable and Soft Electronics Using Liquid Metals. *Adv. Mater.* **2017**, *29*, 1606425.
(31) Lu, B.; Yuk, H.; Lin, S.; Jian, N.; Qu, K.; Xu, J.; Zhao, X. Pure PEDOT: PSS Hydrogels. *Nat. Commun.* **2019**, *10*, 1043.
(32) Feig, V. R.; Tran, H.; Lee, M.; Bao, Z. Mechanically Tunable Conductive Interpenetrating Network Hydrogels That Mimic the Elastic Moduli of Biological Tissue. *Nat. Commun.* **2018**, *9*, 2740.
(33) Sun, J.-Y.; Keplinger, C.; Whitesides, G. M.; Suo, Z. Ionic Skin. *Adv. Mater.* **2014**, *26*, 7608−7614.
(34) Kim, Y.; Zhu, J.; Yeom, B.; Di Prima, M.; Su, X.; Kim, J.-G.; Yoo, S. J.; Uher, C.; Kotov, N. A. Stretchable Nanoparticle Conductors with Self-organized Conductive Pathways. *Nature* **2013**, *500*, 59.
(35) Matsuhisa, N.; Kaltenbrunner, M.; Yokota, T.; Jinno, H.; Kuribara, K.; Sekitani, T.; Someya, T. Printable Elastic Conductors with a High Conductivity for Electronic Textile Applications. *Nat. Commun.* **2015**, *6*, 7461.
(36) Markvicka, E. J.; Bartlett, M. D.; Huang, X.; Majidi, C. An Autonomously Electrically Self-healing Liquid Metal−elastomer Composite for Robust Soft-matter Robotics and Electronics. *Nat. Mater.* **2018**, *17*, 618.
(37) Cattin, C.; Hubert, P. Piezoresistance in Polymer Nanocomposites with High Aspect Ratio Particles. *ACS Appl. Mater. Interfaces* **2014**, *6*, 1804−1811.
(38) Robert, C.; Feller, J. F.; Castro, M. Sensing Skin for Strain Monitoring Made of PC−CNT Conductive Polymer Nanocomposite Sprayed Layer by Layer. *ACS Appl. Mater. Interfaces* **2012**, *4*, 3508−3516.
(39) Xu, R.; Lu, Y.; Jiang, C.; Chen, J.; Mao, P.; Gao, G.; Zhang, L.; Wu, S. Facile Fabrication of Three-Dimensional Graphene Foam/Poly(dimethylsiloxane) Composites and Their Potential Application as Strain Sensor. *ACS Appl. Mater. Interfaces* **2014**, *6*, 13455−13460.
(40) Matsuhisa, N.; Inoue, D.; Zalar, P.; Jin, H.; Matsuba, Y.; Itoh, A.; Yokota, T.; Hashizume, D.; Someya, T. Printable Elastic Conductors by in Situ Formation of Silver Nanoparticles from Silver Flakes. *Nat. Mater.* **2017**, *16*, 834.
(41) Wang, J.; Cai, G.; Li, S.; Gao, D.; Xiong, J.; Lee, P. S. Printable Superelastic Conductors with Extreme Stretchability and Robust Cycling Endurance Enabled by Liquid-metal Particles. *Adv. Mater.* **2018**, *30*, 1706157.
(42) Chun, K.-Y.; Oh, Y.; Rho, J.; Ahn, J.-H.; Kim, Y.-J.; Choi, H. R.; Baik, S. Highly Conductive, Printable and Stretchable Composite Films of Carbon Nanotubes and Silver. *Nat. Nanotechnol.* **2010**, *5*, 853.
(43) Sekitani, T.; Noguchi, Y.; Hata, K.; Fukushima, T.; Aida, T.; Someya, T. A Rubberlike Stretchable Active Matrix Using Elastic Conductors. *Science* **2008**, *321*, 1468−1472.
(44) Oh, J. Y.; Lee, D.; Hong, S. H. Ice-Templated Bimodal-Porous Silver Nanowire/PDMS Nanocomposites for Stretchable Conductor. *ACS Appl. Mater. Interfaces* **2018**, *10*, 21666−21671.
(45) Liu, J.; Guo, Q.; Mao, S.; Chen, Z.; Zhang, X.; Yang, Y.; Zhang, X. Templated Synthesis of a 1D Ag Nanohybrid in the Solid State and Its Organized Network for Strain-Sensing Applications. *J. Mater. Chem. C* **2018**, *6*, 10730−10738.
(46) Hu, Y.; Zhao, T.; Zhu, P.; Zhu, Y.; Shuai, X.; Liang, X.; Sun, R.; Lu, D. D.; Wong, C.-P. Low Cost and Highly Conductive Elastic Composites for Flexible and Printable Electronics. *J. Mater. Chem. C* **2016**, *4*, 5839−5848.
(47) Hu, Y.; Zhao, T.; Zhu, P.; Zhang, Y.; Liang, X.; Sun, R.; Wong, C. P. A Low-cost, Printable, and Stretchable Strain Sensor Based on Highly Conductive Elastic Composites with Tunable Sensitivity for Human Motion Monitoring. *Nano Res.* **2018**, *11*, 1938−1955.
(48) Niu, X. Z.; Peng, S. L.; Liu, L. Y.; Wen, W. J.; Sheng, P. Characterizing and Patterning of PDMS-Based Conducting Composites. *Adv. Mater.* **2007**, *19*, 2682−2686.
(49) Larmagnac, A.; Eggenberger, S.; Janossy, H.; Vörös, J. Stretchable Electronics Based on Ag-PDMS Composites. *Sci. Rep.* **2014**, *4*, 7254.
(50) Chu, K.; Lee, S.-C.; Lee, S.; Kim, D.; Moon, C.; Park, S.-H. Smart Conducting Polymer Composites Having Zero Temperature Coefficient of Resistance. *Nanoscale* **2015**, *7*, 471−478.
(51) Gong, S.; Wu, D.; Li, Y.; Jin, M.; Xiao, T.; Wang, Y.; Xiao, Z.; Zhu, Z.; Li, Z. Temperature-independent Piezoresistive Sensors Based on Carbon Nanotube/Polymer Nanocomposite. *Carbon* **2018**, *137*, 188−195.

DOI: 10.1021/acsami.9b13266
ACS Appl. Mater. Interfaces 2019, 11, 42561−42570

(52) Chu, K.; Park, S.-H. Fabrication of a Hybrid Carbon-Based Composite for Flexible Heating Element With a Zero Temperature Coefficient of Resistance. *IEEE Electron Device Lett.* **2015**, *36*, 50−52.
(53) Hellebrekers, T.; Ozutemiz, K. B.; Yin, J.; Majidi, C. Liquid Metal-Microelectronics Integration for a Sensorized Soft Robot Skin. In *2018 IEEE/RSJ International Conference on Intelligent Robots and Systems (IROS)*; IEEE: 1−5 Oct. 2018, 5924−5929.

DOI: 10.1021/acsami.9b13266
ACS Appl. Mater. Interfaces 2019, 11, 42561−42570